Supporting Information for

CO_2 Reduction to CO with 19 % Efficiency in a Solar-Driven Gas Diffusion Electrode Flow Cell under Outdoor Solar Illumination

Wen-Hui Cheng[1], Matthias H. Richter[2], Ian Sullivan[2], David M. Larson[3],

Chengxiang Xiang[2], Bruce S. Brunschwig[4]*, Harry A. Atwater[1]*

[1] Department of Applied Physics and Material Science, California Institute of Technology, Pasadena, CA 91125, USA.

[2] Division of Chemistry and Chemical Engineering, California Institute of Technology, Pasadena, CA 91125, USA.

[3] Chemical Sciences Division, Lawrence Berkeley National Laboratory, Berkeley, CA 94720, USA.

[4] Beckman Institute, California Institute of Technology, Pasadena, CA 91125, USA.

correspondence to: bsb@caltech.edu, haa@caltech.edu

This PDF file includes:

Methods

Gas diffusion electrode preparation

GDEs were prepared with diluted Ag-NPs (Sigma Aldrich 736481, particle diameter ≤50 nm, 30-35 wt. % in triethylene glycol monoethyl ether) by drop-casting on carbon paper (Sigracet 29 BC). 50 μL of Ag-NPs ink was diluted with 15 mL of methanol and sonicated prior to use. 200 μL of the diluted Ag-NPs were drop-casted on 25 mm by 25 mm size carbon paper (masked to A_{GDE} = 0.31 cm^2 later for operation). The GDE was baked at ~100 ˚C for 10 min on a hot plate to remove the remaining solvent and was post annealed at 200 °C for 1 h in a muffle furnace in air. Surface chemical analysis was conducted using X-ray photoelectron spectroscopy (XPS) with the catalyst primarily in a metallic phase (Figure S6).

Electrochemical measurements of GDE cell

A PEEK compression cell (Figure 1a, Figure S1) was used as the vessel for the measurement with anode and cathode chamber volumes of 2 mL. The anode and cathode electrode working areas were 0.31 cm^2, and the membrane area was 2.4 cm^2 as constrained by the design of the compression cell. 1 M potassium hydroxide (KOH) was used as the catholyte for experiments at pH 14, while 1 M potassium bicarbonate ($KHCO_3$) buffer was used for pH 8.5. The anolyte was 1 M KOH. The corresponding anion exchange membrane (AEM) was a Fumasep FAA-3-50 for alkaline environments and a Selemion AMV for neutral environment. The anode was a Pt foil under three-electrode operation, while for full cell operation in KOH electrolyte we used Ni foam to reduce the overpotential for oxygen evolution reaction. A leakless Ag/AgCl reference electrode was used for three-electrode measurements and to determine the GDE potential in the two-electrode measurements. All electrochemical measurements were performed using a Biologic VSP-300 potentiostat. Scan rates were set to 50 $mV \cdot s^{-1}$. A Keithley 2000 multimeter was used to record the cell voltage and a Keithley 2182A nanovoltmeter for recording the voltage between the cathode and reference electrode. Gas flow rates of the flow controller (Gas inlet) and flow meter (Gas outlet) where recorded by the external device inputs of the potentiostat.

Gas supply and detection

The electrochemical setup was operated in a continuous flow mode. Carbon dioxide was provided to the electrochemical cell and its flow rate was controlled with an Alicat flow controller. The carbon dioxide stream could be supplied either as dry gas or humidified CO_2 with a gas bubbler between the cell and flow controller. The exhaust gasses went through a liquid trap than an Alicat flow meter, and finally to a gas chromatograph (SRI-8610) using a Hayesep D column and a Molsieve 5A column with N_2 as the carrier gas. The gaseous products were detected using a thermal conductivity detector (TCD) and a flame ionization detector (FID) equipped with a methanizer. Quantitative analysis of gaseous products was based on calibration with several gas standards over many orders of magnitude in concentration.

PV-GDE integration and measurements

The GaInP/GaInAs/Ge triple junction cell is commercially available from Spectrolab (C4MJ) with geometric area of 0.31 cm^2. The solid-state J-V characteristic and performance parameters of the solar cell are shown in Figure S4.

For illumination during laboratory tests, an Oriel Instruments 75 W Solar Simulator was used, the lamp spectrum matching with AM 1.5G is presented in Figure S5 and Table S2. The response to natural sunlight of the triple junction at short circuit was calibrated by measuring the outdoor sunlight irradiance with a calibrated Si photodiode. The light intensity of the solar simulator was set to provide same short circuit current from the InP/GaInAs/Ge triple junction cell as it would under AM 1.5G outdoor sunlight. While this is not expected to yield a simulated solar irradiance of 100 $mW \cdot cm^{-2}$ due to the different solar irradiance in the 800–1000 and 1150–1800 nm regions it does produce a response of the triple junction PV that is the same as it would in actual AM 1.5G sunlight. The corresponding sub-cell currents with integration of external quantum efficiency and short circuit current over the two illumination spectra are shown in Table S2.

For outdoor tests the triple junction solar cell was mounted on a solar tracker, see illustration in Fig S8. An Arduino microcontroller was used to control the solar tracker and measure the sun light intensity through a calibrated (350 to 1100 nm, 1 cm^2) NIST traceable Si photodiode (Thorlabs FDS1010-CAL).

Surface analyses

Kratos Axis Ultra was used to perform X-ray photoelectron spectroscopy (XPS) measurements with base pressure under $1x10^{-9}$ Torr. A monochromatic Al Kα ($\hbar\omega$ = 1486.69 eV) source with a power of 150 W was used for all measurements. A ramé-hart contact angle goniometer was used for surface angle measurement. The images were analyzed with ImageJ with the help of the Drop Analysis' plugin developed at the École polytechnique fédérale de Lausanne (EPFL).

Solar-to-fuel efficiency:

Solar-to-fuel efficiency is defined as:

$$\eta_{\mathrm{STF}} = \frac{\mathrm{P_{out}}}{\mathrm{P_{in}}} = \frac{J_{\mathrm{GDE}} \cdot \Delta U_{\mathrm{rxn}} \cdot f_{FE,CO.} \cdot A_{\mathrm{GDE}}}{\mathrm{C} \cdot P_{\mathrm{light}} \cdot A_{\mathrm{PV}}} = \frac{J_{\mathrm{GDE}} \cdot 1.34\mathrm{V} \cdot f_{\mathrm{FE,CO}} \cdot A_{\mathrm{GDE}}}{\mathrm{C} \cdot P_{\mathrm{light}} \cdot A_{\mathrm{PV}}} \quad \text{(S1)}$$

Where J_{GDE} is the current density (mA·cm^{-2}) of the GDE, ΔU_{rxn} is the thermodynamic potential (V) for the overall reaction, $f_{\mathrm{FE,CO}}$ is the Faradaic efficiency, C is light concentration factor, P_{light} is the incident light irradiance (mW·cm^{-2}) before concentration, and A_{GDE} and A_{PV} are the areas of the GDE and PV (cm^2), respectively. For CO_2 to CO as the cathodic reaction and H_2O to oxygen evolution reaction on the anode ΔU_{rxn} is 1.34 V.

For our device with A_{GDE} = A_{PV} = 0.31 cm^2 under 1sun AM 1.5G illumination, C = 1, we obtained:

$$\eta_{\mathrm{STF}} = \frac{J_{\mathrm{GDE}} \cdot 1.34\mathrm{V} \cdot f_{\mathrm{FE,CO}}}{P_{\mathrm{light}}} = \frac{14.4\frac{\mathrm{mA}}{\mathrm{cm}^2} \cdot 1.34\mathrm{V} \cdot 0.989}{100\frac{\mathrm{mW}}{\mathrm{cm}^2}} = 19.1\% \quad \text{(S2)}$$

Under concentrated solar illumination (C = 3.25, A_{GDE} = 1 cm^2, A_{PV} = 0.31 cm^2) the efficiency of the device was:

$$\eta_{\mathrm{STF}} = \frac{J_{\mathrm{GDE}} \cdot 1.34\mathrm{V} \cdot f_{\mathrm{FE,CO}}}{3.25 \cdot P_{\mathrm{light}} \cdot 0.31\mathrm{cm}^2} = \frac{14.6\frac{\mathrm{mA}}{\mathrm{cm}^2} \cdot 1.34\mathrm{V} \cdot 0.962}{3.25 \cdot 100\frac{\mathrm{mW}}{\mathrm{cm}^2} \cdot 0.31\mathrm{cm}^2} = 18.7\% \quad \text{(S3)}$$

Since $J_{\mathrm{GDE}} \cdot A_{\mathrm{GDE}} = J_{\mathrm{PV}} \cdot A_{\mathrm{PV}}$, equation S3 can also be rewritten using J_{PV}:

$$\eta_{\mathrm{STF}} = \frac{J_{\mathrm{PV}} \cdot \Delta U_{\mathrm{rxn}} \cdot f_{FE,CO.}}{\mathrm{C} \cdot P_{\mathrm{light}}} = \frac{47.1\frac{\mathrm{mA}}{\mathrm{cm}^2} \cdot 1.34\mathrm{V} \cdot 0.962}{3.25 \cdot 100\frac{\mathrm{mW}}{\mathrm{cm}^2}} = 18.7\% \quad \text{(S4)}$$

In order to maximize the solar-to-fuel efficiency for a specific PV component which can provide enough voltage for the reaction, the operation point, defined as the intersection of PV *J-U* and GDE *J-U* curve, needs to be tuned for the maximum of $J_{\mathrm{PV}} \cdot f_{\mathrm{FE}}$.

Once this condition is fulfilled, the actual cell voltage and energy efficiency of the GDE device can be calculated. The energy efficiency of the GDE is defined as:

$$\eta_{\mathrm{GDE}} = \frac{P_{out}}{P_{in}} = \frac{\Delta U_{\mathrm{rxn}} \cdot J_{\mathrm{GDE}} \cdot A_{\mathrm{GDE}} \cdot f_{FE,CO.}}{U_{cell} \cdot J_{\mathrm{PV}} \cdot A_{\mathrm{PV}}} = \frac{\Delta U_{\mathrm{rxn}} \cdot f_{FE,CO.}}{U_{cell}} \quad \text{(S5)}$$

Calculation of turnover frequency (TOF):

Turnover frequency (TOF) was defined as the CO production rate (in moles cm^{-1} h^{-1}) divided by the number of moles of active site catalyst. Consider the 0.26 $mmol \cdot h^{-1} \cdot cm^{-2}$ (7.4 $mg \cdot h^{-1} \cdot cm^{-2}$) CO production rate per catalyst area at -0.6 V vs RHE. The total catalyst loading was 0.001 $mmol \cdot cm^{-2}$ (0.12 $mg \cdot cm^{-2}$) that gave a TOF based on the total amount of Ag-NPs as 260 h^{-1}. Since only the surface atoms of the nanoparticle can contribute to active sites, we estimate the fraction of surface atoms of a 50 nm diameter Ag nanoparticle to be ~3 %, then the moles of active sites is $\sim 3 \times 10^{-5}$ mmol cm^{-2} and the TOF based on the number of surface atoms is $\sim 9 \times 10^3$ h^{-1}.

Definition of potential:

A leakless Ag/AgCl (sat.) reference electrode was used for three-electrode measurements and to determine the GDE potential in the two-electrode measurements. To convert from from the potential vs. Ag/AgCl to vs. NHE and vs. RHE equation S6 and S7 are used.

$$U_{Ag/AgCl} = U_{NHE} + 0.197V \quad \text{(S6)}$$

$$U_{RHE} = U_{NHE} + 0.0591V \times pH = U_{Ag/AgCl} + 0.197V + 0.0591V \times pH \quad \text{(S7)}$$

To obtain the potential of the GDE (U_{GDE}) vs. RHE the measured potential vs. Ag/AgCl was corrected for 1 M $KHCO_3$ (pH = 8.5)

$$U_{GDE,RHE} = U_{GDE,Ag/AgCl} + 0.197V + 0.0591V \times 8.5 = U_{GDE,Ag/AgCl} + 0.699V \quad \text{(S8)}$$

and 1 M KOH (pH =14)

$$U_{GDE,RHE} = U_{GDE,Ag/AgCl} + 0.197V + 0.0591V \times 14 = U_{GDE,Ag/AgCl} + 1.024V \quad \text{(S9)}$$

The overpotential of the GDE is defined as the difference of applied potential to the thermodynamic potential of CO_2 to CO on the RHE scale (–0.11 V vs RHE).

$$Overpotential = |U_{GDE,RHE} + 0.11V| \quad \text{(S10)}$$

Calculation of CO_2 loss to KOH neutralization:

The volume of the catolyte was 0.5 L 1 M KOH (0.5 mol KOH) with an initial pH of 14 which changed to 13.7 after 150 h of continuous operation. A pH of 13.7 is $10^{13.7-14}$M KOH $= 0.5$ M KOH which for 0.5 L is 0.25 mol KOH.

The reaction of KOH and CO_2 is given by equation S11.

$$2KOH + CO_2 = K_2CO_3 + H_2O \quad \text{(S11)}$$

A loss of 0.25 mol KOH corresponds to a loss of 0.125 mol CO_2 and formation of equal amount (0.125 mol) K_2CO_3. The CO_2 flowrate during the experiment was 10 sccm which over 150 h corresponds to 4.043 mol CO_2. The total percentage of CO_2 lost to KOH neutralization and carbonate formation is then $\frac{0.125}{4.043} = 0.031 \equiv 3.1\ \%$.

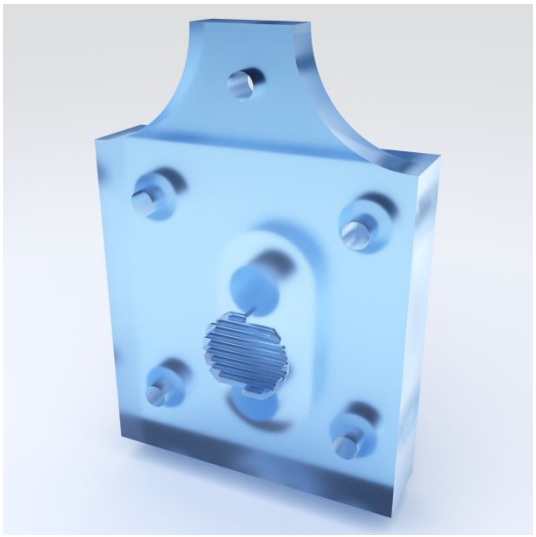

Figure S1. Backplate as shown in Figure 1a item 5 with an interdigitated flow field.

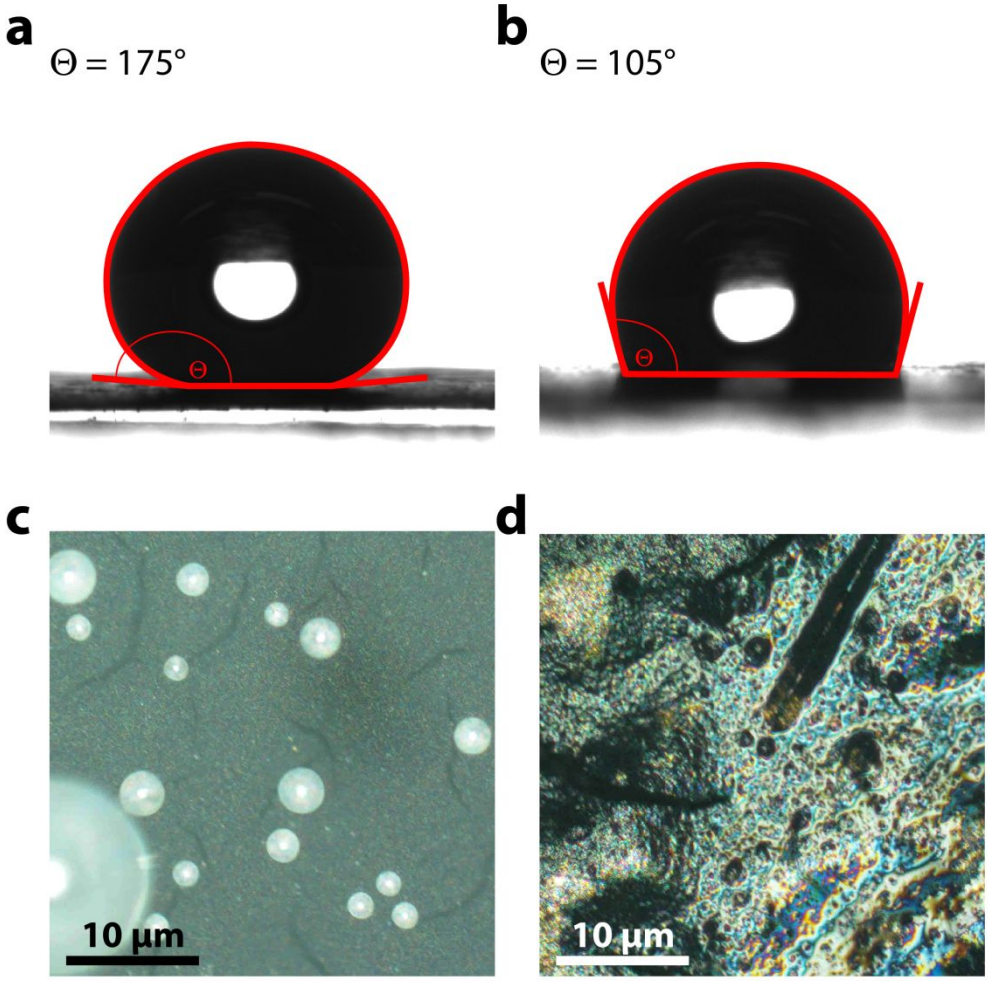

Figure S2. Contact angle Θ measurement of water on **a** pristine Sigracet 29 BC carbon paper and **b** with Ag-NPs on Sigracet 29BC carbon paper after electrolysis. The contact angle is 175° for **a** and 105° for **b**. Optical micrographs of water pushing through the back of the Sigracet 29 BC carbon paper **c** without Ag-NPs and **d** with Ag-NPs. The formation of small liquid bubbles is observed in **c** while a thin water layer is shown in **d** indicating the catalyst surface is wetted during operation as proposed.

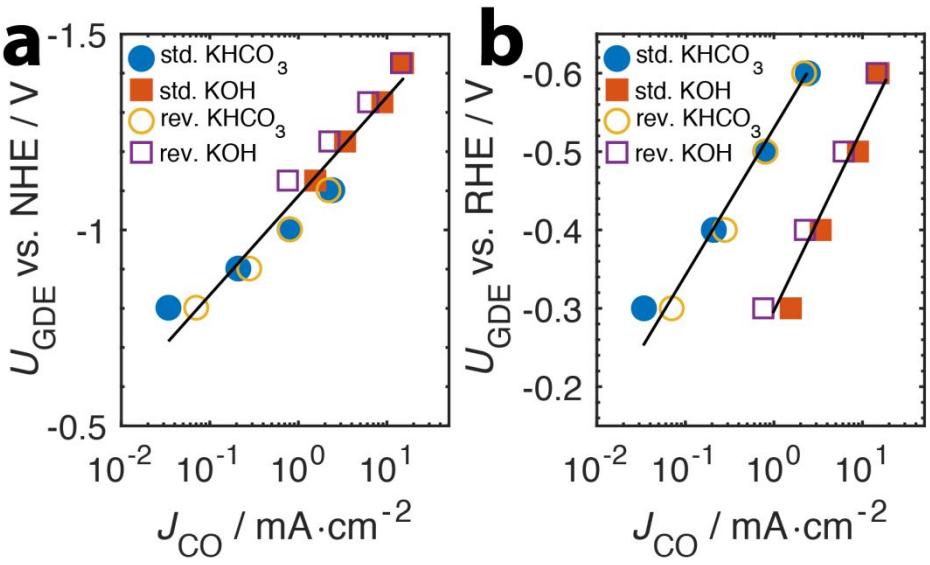

Figure S3. a GDE potential vs. NHE, **b** GDE potential vs. RHE versus CO partial current of Ag-NP GDE (rev. indicating reserve-assembled, std. indicating standard-assembled) for CO_2 reduction to CO in 1 M $KHCO_3$ and 1 M KOH.

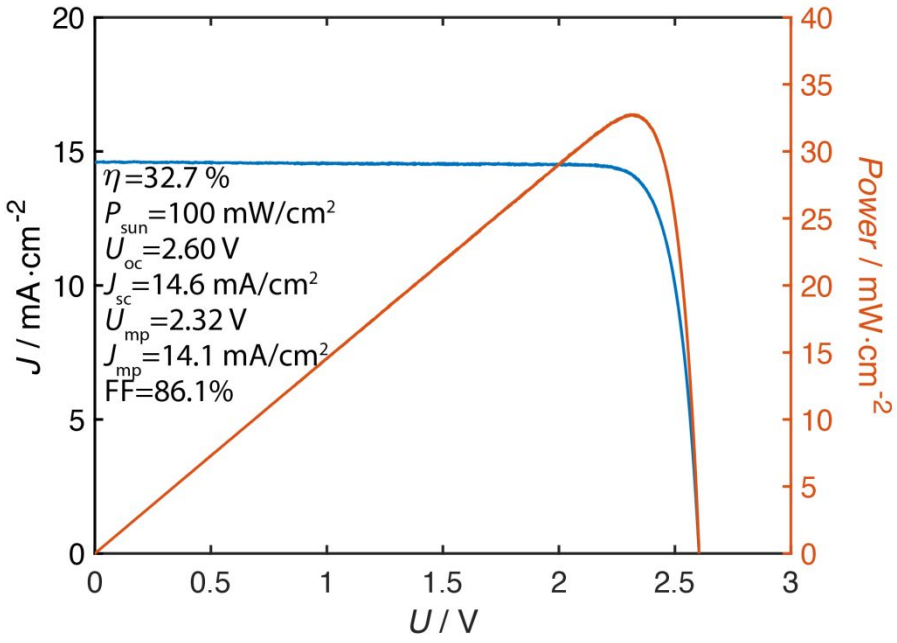

Figure S4. J-V characteristic of the GaInP/GaInAs/Ge triple junction cell. U_{oc} is the open circuit voltage, J_{sc} the short circuit current, U_{mp}/J_{mp} the current and voltage at the maximum power point, and FF the fill factor.

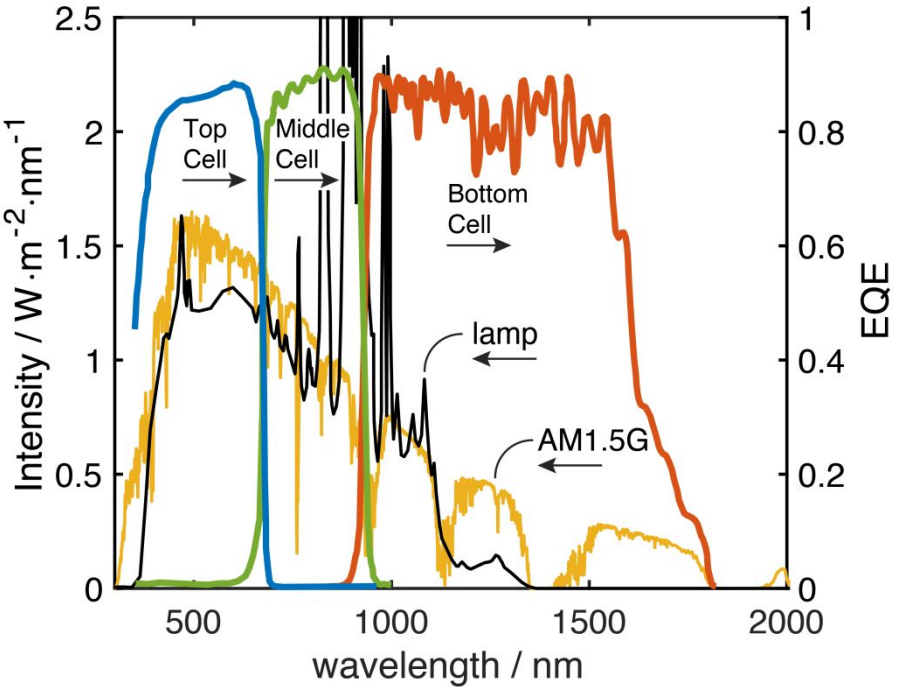

Figure S5. Intensity (left axis) of AM 1.5G 1 sun reference spectrum (gold) and solar simulator spectrum (black), external quantum efficiency (right axis) of the GaInP/GaInAs/Ge (blue, green, red) triple junction cell.

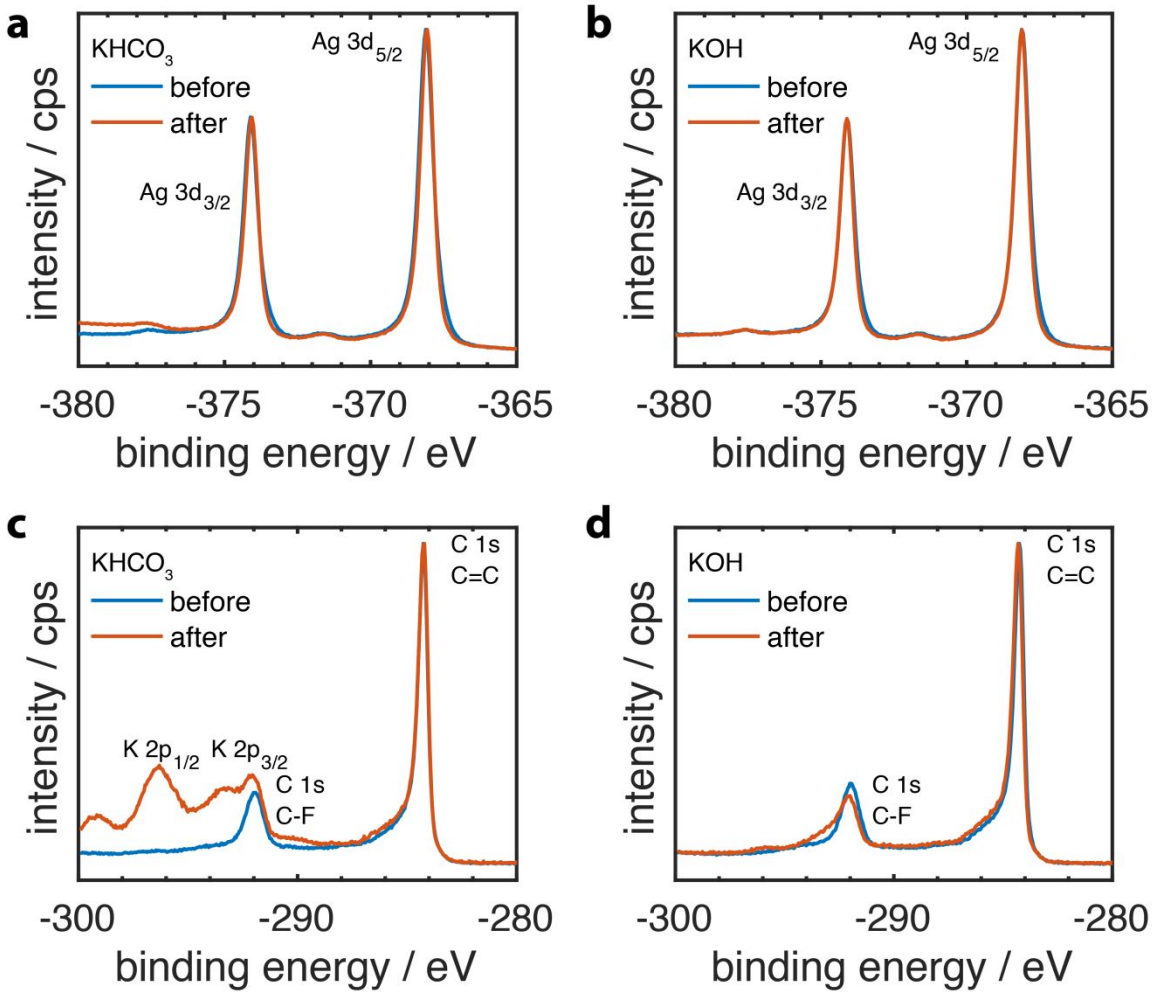

Figure S6. Carbon 1s (C 1s) and Silver 3d (Ag 3d) X-ray photoelectron spectra of Ag-NP GDE before/after electrocatalysis with an electrolyte of **a, c** 1 M $KHCO_3$; **b, d** 1 M KOH.

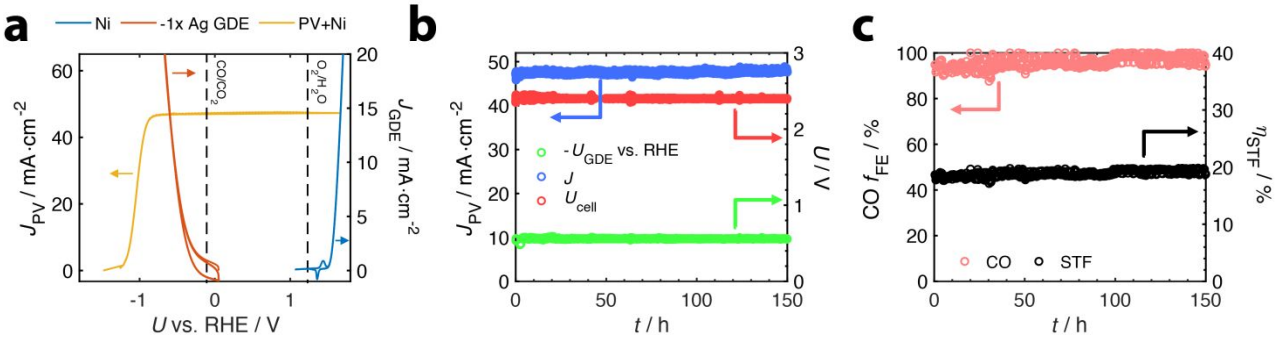

Figure S7. Efficiency and stability assessment at a solar concentration 3.25 Suns. ($C = 3.25$, $A_{GDE} = 1$ cm^2, $A_{PV} = 0.31$ cm^2) **a** *J-U* characteristic of Ni anode, solar cell with Ni anode, and Ag-NP gas diffusion cathode under 3.25 Suns. **b** Current and cell voltage measurement over 150 h duration. **c** The corresponding CO Faradaic efficiency and solar to fuel efficiency over the same 150 h duration.

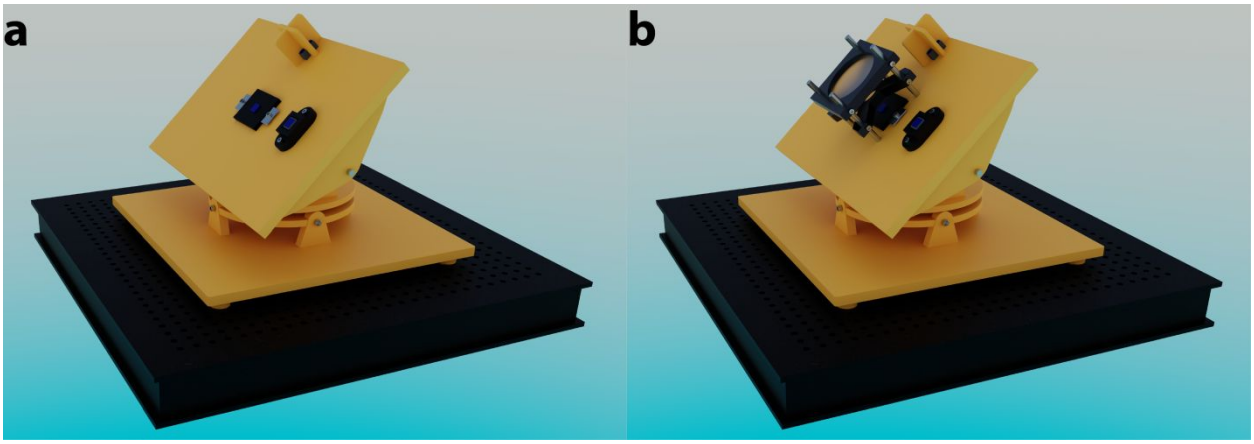

Figure S8. a Illustration of the solar tracker. **b** With the addition of $C = 3.25$ Suns solar concentrator. The PV element is located in the left with a silicon reference photodiode mounted on the right. Above the PV element is the light-dependent resistor sensor array for determining and tracking the position of the sun. For concentrator operation, a Fresnel lens with 51 mm focal length was placed in front of the solar cell to provide a concentration of 3.25x.

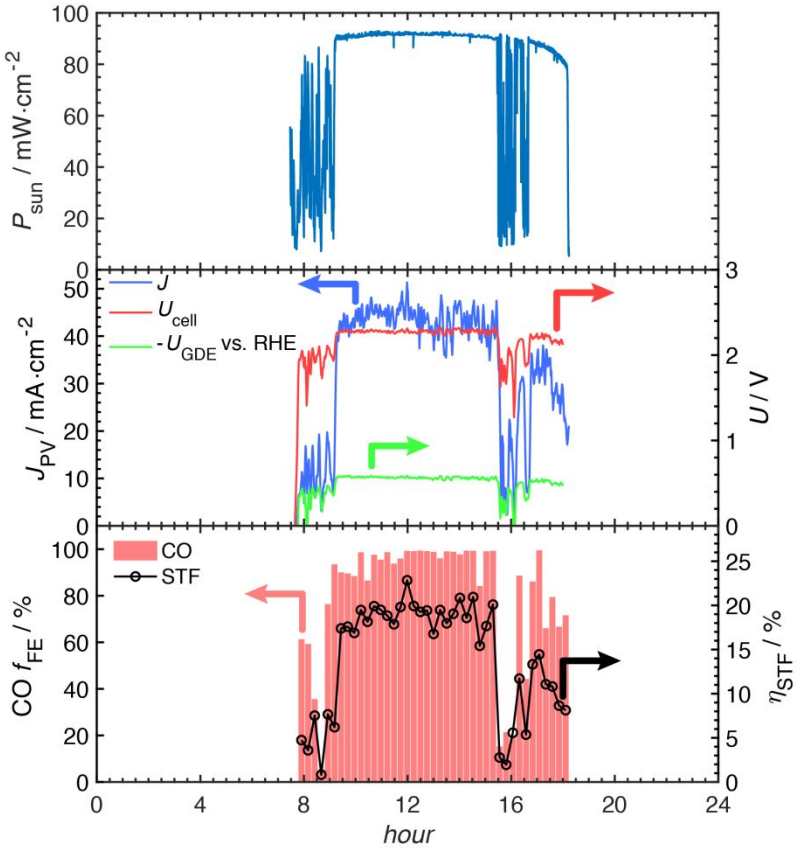

Figure S9. Outdoor tests of solar-driven PV-GDE in Pasadena, CA. The solar irradiance was monitored with a calibrated silicon photodiode. PV operation current J_{PV}, cell voltage U_{cell}, working electrode potential U_{GDE}, CO Faradaic *efficiency* $f_{FE,CO}$ and solar to fuel efficiency η_{STF} were recorded for a 24h day cycle with 3.25x solar concentrator ($C = 3.25$, $A_{GDE} = 1$ cm^2, $A_{PV} = 0.31$ cm^2)

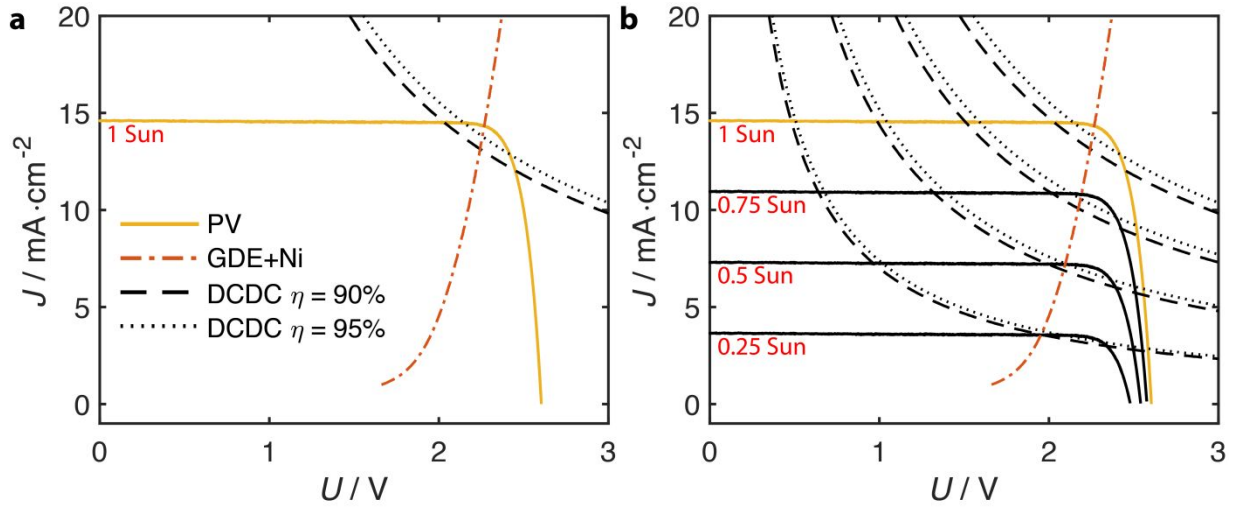

Figure S10. *J-U* characteristic of the GaInP/GaInAs/Ge triple junction cell under 1 Sun (yellow solid line) with combined load curve of Ni anode and Ag GDE cathode (red dot-dashed line) in addition to DC-DC converter output curves (solid PV curve as input) with converter efficiency of 90 % (black dashed line) and 95 % (black dotted line). The PV curves for lower illumination conditions are included on the right figure. The operation point for the directly driven PV-GDE cell is $U_{cell} = 2.23$ V, $J = 14.4$ mA·cm^{-2} with a maximum efficiency of 19.3 %; with an 95 % efficient DC-DC converter the operation point would be $U_{cell} = 2.22$ V, $J = 13.8$ mA·cm^{-2} with a maximum efficiency of 18.5 %; and for a 90 % efficient DC-DC converter the operation point is $U_{cell} = 2.20$ V, $J = 13.2$ mA·cm^{-2} with a maximum efficiency of 17.7 % (maximum efficiency calculated assuming 100 % Faradic efficiency).

Table S1. Comparison of the CO_2 reduction performance of our Ag-NP catalyst with previously reported Ag and Au electrodes. (U as overpotential vs. $E^0_{CO/CO2}$ (-0.11 V vs. RHE), mass activity define as $\frac{J \cdot f_{FE}}{\text{loading}}$)

Catalysts	Electrolyte	pH	U (V) at ~15 mA·cm^{-2}	$f_{FE,CO}$ (%)	Loading (mg·cm^{-2})	Mass activity (mA·mg^{-1})	Ref.
Nanoporous Au	CO_2-sat 0.2 M $KHCO_3$	6.8	1.24	N/A	0.39 (200 nm film)	N/A	1
Nanoporous Au	CO_2-sat 0.1 M $KHCO_3$	6.8	0.6	60	0.47 (eq. 240 nm film)	19.15	2
OD-Au	CO_2-sat 0.5 M $NaHCO_3$	7.2	0.39	100	193 (0.1 mm foil)	0.08	3
Au-NWs	CO_2-sat 0.5 M $KHCO_3$	7.2	0.32	90	4.43	3.05	4
Au nanoneedle	CO_2-sat 0.5 M $KHCO_3$	7.4	0.24	95	N/A	N/A	5
Bilayer Au/PE	CO_2-sat 0.5 M $KHCO_3$ flow cell	7.2	0.39	85	0.15	85	6
Au-NPs	2M KOH flow cell	13.77	0.2	70	0.18	58.33	7
Polycrystalline Ag	CO_2-sat 0.1 M $KHCO_3$	6.8	1.4	30	105 (0.1 mm foil)	0.04	8
Polycrystalline Ag	CO_2-sat 0.5 M $KHCO_3$	7.0	1.04	60	N/A (foil)	N/A	9
5 nm Ag/C	CO_2-sat 0.5 M $KHCO_3$	7.0	0.84	40	0.09	66.67	9
Ag-NPs	CO_2-sat 0.1 M $KHCO_3$	6.8	0.84	83	N/A	N/A	10
cysteamine-capped Ag-NPs	CO_2-sat 0.5 M $NaHCO_3$	7.2	0.69	66	0.08	123.75	11
Ag Nano-coarals	CO_2-sat 0.1 M $KHCO_3$	6.8	0.61	95	N/A (on foil)	N/A	12
Nanoporous Ag	CO_2-sat 0.5 M $KHCO_3$	7.2	0.49	92	40	0.35	13

Ag/PTFE	1 M $KHCO_3$ flow cell	8.5	0.64	70	0.52 (eq. 500 nm film)	20.19	14
Ag-NPs	1M KOH flow cell	14	0.39	95	1	14.25	15
Ag/PTFE	1M KOH flow cell	14	0.34	90	0.52 (eq. 500 nm film)	25.96	14
Ag-NPs	0.5M KOH flow cell	13.23	0.34	95	2	7.125	16
Ag-NPs	1M KOH flow cell	14	0.49	99	0.12	124	This work

Table S2. Currents calculated for the individual sub-cells of the of the GaInP/GaInAs/Ge triple junction PV cell under 1.5G 1 sun illumination assuming the standard reference sunlight spectrum (AM1.5G ASTM G-173 reference spectrum was taken from the Renewable Resource Data Center (RReDC) of the National Renewable Energy Laboratory (NREL)) or the solar simulator spectrum and measured short circuit photocurrent J_{sc} under respective 1 sun conditions.

Illumination Source	J_{GaInP} **(mA·cm^{-2})**	J_{GaInAs} **(mA·cm^{-2})**	J_{Ge} **(mA·cm^{-2})**	J_{sc} **(mA·cm^{-2})**
AM 1.5G	15.56	14.83	18.53	14.6
Solar simulator	15.32	29.73	14.83	14.6

Table S3. Comparison of the PV-GDE performance studied herein with different measurement conditions and calculations.

Irradiance ($mW \cdot cm^{-2}$)	Source	A_{PV} (cm^2)	A_{GDE} (cm^2)	$f_{FE,CO}$ (%)	η_{GDE} (%)	η_{STF} (%)	J_{PV} ($mA \cdot cm^{-2}$)	U_{cell} (V)	Power ($mW \cdot cm^{-2}$)
100	Simulated	0.31	0.31	99	59.4	19.1	14.4	2.23	32.1
325	Simulated	0.31	1	96	53.7	18.9	47.5	2.39	113.5
91	Natural	0.31	0.31	96	58.5	18.7	13.0	2.20	28.6
296	Natural	0.31	1	96	55.9	18.9	43.0	2.30	98.9
100	Calculated	0.31	0.31	100	60.0	19.3	14.4	2.23	32.1
100	Calculated	0.31	0.31	100	60.4	18.5	13.8	2.22	30.6
100	Calculated	0.31	0.31	100	60.9	17.7	13.2	2.20	29.0

Table S4. Comparison of the performance of the PV-GDE studied herein with the current state of the art PV-electrolyzer for CO_2 reduction to CO.[17]

	Current record [17]	This work
Solar-to-CO (%)	13.4	**19.1**
PV size (cm^2)	0.563	0.31
Cathode / Anode	both SnO_2 / CuO	Ag GDE / Ni foil
Cathode & Anode size (cm^2)	20	0.31
Catholyte / Membrane / Anolyte	0.25 M CsOH / BPM / CO_2-sat 0.1 M $CsHCO_3$	1 M KOH /AEM / 1 M KOH
Operation current (mA)	6.6	4.5
$f_{FE,CO}$ (%)	86	99
CO production rate ($mg \cdot h^{-1} \cdot cm^{-2}$)	0.145	**7.4**
CO production rate outdoor (mg/day)	-	**15 (50 at 3.25 Suns)**
Stability (h)	5 (with 15% loss)	**20 (150 h at 3.25 Suns)**

References

(1) Song, J. T.; Ryoo, H.; Cho, M.; Kim, J.; Kim, J.-G.; Chung, S.-Y.; Oh, J. Nanoporous Au Thin Films on Si Photoelectrodes for Selective and Efficient Photoelectrochemical CO_2 Reduction. *Adv Energy Mater* **2017**, *7* (3), 1601103.

(2) Welch, A. J.; DuChene, J. S.; Tagliabue, G.; Davoyan, A.; Cheng, W.-H.; Atwater, H. A. Nanoporous Gold as a Highly Selective and Active Carbon Dioxide Reduction Catalyst. *ACS Appl. Energy Mater.* **2018**, *2* (1), 164–170.

(3) Chen, Y.; Li, C. W.; Kanan, M. W. Aqueous CO_2 Reduction at Very Low Overpotential on Oxide-Derived Au Nanoparticles. *J. Am. Chem. Soc.* **2012**, *134* (49), 19969–19972.

(4) Zhu, W.; Zhang, Y.-J.; Zhang, H.; Lv, H.; Li, Q.; Michalsky, R.; Peterson, A. A.; Sun, S. Active and Selective Conversion of CO_2 To CO on Ultrathin Au Nanowires. *J. Am. Chem. Soc.* **2014**, *136* (46), 16132–16135.

(5) Liu, M.; Pang, Y.; Zhang, B.; De Luna, P.; Voznyy, O.; Xu, J.; Zheng, X.; Dinh, C. T.; Fan, F.; Cao, C.; de Arquer, F. P. G.; Safaei, T. S.; Mepham, A.; Klinkova, A.; Kumacheva, E.; Filleter, T.; Sinton, D.; Kelley, S. O.; Sargent, E. H. Enhanced Electrocatalytic CO_2 Reduction via Field-Induced Reagent Concentration. *Nature* **2016**, *537* (7620), 382–386.

(6) Li, J.; Chen, G.; Zhu, Y.; Liang, Z.; Pei, A.; Wu, C.-L.; Wang, H.; Lee, H. R.; Liu, K.; Chu, S.; Cui, Y. Efficient Electrocatalytic CO_2 Reduction on a Three-Phase Interface. *Nature Catalysis* **2018**, *1* (8), 592–600.

(7) Insights Into the Low Overpotential Electroreduction of CO_2 To CO on a Supported Gold Catalyst in an Alkaline Flow Electrolyzer. *ACS Energy Lett.* **2017**, 193–198.

(8) Clark, E. L.; Resasco, J.; Landers, A.; Lin, J.; Chung, L.-T.; Walton, A.; Hahn, C.; Jaramillo, T. F.; Bell, A. T. Standards and Protocols for Data Acquisition and Reporting for Studies of the Electrochemical Reduction of Carbon Dioxide. *ACS Catal* **2018**, *8* (7), 6560–6570.

(9) Kim, C.; Jeon, H. S.; Eom, T.; Jee, M. S.; Kim, H.; Friend, C. M.; Min, B. K.; Hwang, Y. J. Achieving Selective and Efficient Electrocatalytic Activity for CO_2 Reduction Using Immobilized Silver Nanoparticles. *J. Am. Chem. Soc.* **2015**, *137* (43), 13844–13850.

(10) Jiang, K.; Kharel, P.; Peng, Y.; Gangishetty, M. K.; Lin, H.-Y. G.; Stavitski, E.; Attenkofer, K.; Wang, H. Silver Nanoparticles with Surface-Bonded Oxygen for Highly Selective CO_2 Reduction. *ACS Sustainable Chem. Eng.* **2017**, *5* (10), 8529–8534.

(11) Wang, Z.; Wu, L.; Sun, K.; Chen, T.; Jiang, Z.; Cheng, T.; William A Goddard, I. Surface Ligand Promotion of Carbon Dioxide Reduction Through Stabilizing Chemisorbed Reactive Intermediates. *J Phys Chem C* **2018**, *9* (11), 3057–3061.

(12) Hsieh, Y.-C.; Senanayake, S. D.; Zhang, Y.; Xu, W.; Polyansky, D. E. Effect of Chloride Anions on the Synthesis and Enhanced Catalytic Activity of Silver Nanocoral Electrodes for CO_2 Electroreduction. *ACS Catal* **2015**, *5* (9), 5349–5356.

(13) Lu, Q.; Rosen, J.; Zhou, Y.; Hutchings, G. S.; Kimmel, Y. C.; Chen, J. G.; Jiao, F. A Selective and Efficient Electrocatalyst for Carbon Dioxide Reduction. *Nat. Commun.* **2014**, *5*, 3242.

(14) Dinh, C. T.; Garcia de Arquer, F. P.; Sinton, D.; Sargent, E. H. High Rate, Selective, and Stable Electroreduction of CO_2 to CO in Basic and Neutral Media. *ACS Energy Lett.* **2018**, *3* (11), 2835–2840.

(15) Tornow, C. E.; Thorson, M. R.; Ma, S.; Gewirth, A. A.; Kenis, P. J. A. Nitrogen-Based Catalysts for the Electrochemical Reduction of CO_2 To CO. *J. Am. Chem. Soc.* **2012**, *134* (48), 19520–19523.
(16) Verma, S.; Lu, X.; Ma, S.; Masel, R. I.; Kenis, P. J. A. The Effect of Electrolyte Composition on the Electroreduction of CO_2 To CO on Ag Based Gas Diffusion Electrodes. *Phys. Chem. Chem. Phys.* **2016**, *18* (10), 7075–7084.
(17) Schreier, M.; Héroguel, F.; Steier, L.; Ahmad, S.; Luterbacher, J. S.; Mayer, M. T.; Luo, J.; Grätzel, M. Solar Conversion of CO_2 To CO Using Earth-Abundant Electrocatalysts Prepared by Atomic Layer Modification of CuO. *Nature Energy* **2017**, *2* (7), 17087.